# Distribution over pore radii in random and isotropic systems of polydisperse rods with finite aspect ratios

Avik P. Chatterjee*

*Department of Chemistry, SUNY College of Environmental Science and Forestry, One Forestry Drive, Syracuse, New York 13210, USA*

(Received 31 March 2016; revised manuscript received 3 May 2016; published 3 June 2016)

Excluded-volume arguments are applied toward modeling the pore-size distribution in systems of randomly arranged cylindrical rods with finite and nonuniform aspect ratios. An explicit expression for the pore-size distribution is obtained by way of an analogy to a hypothetical system of fully penetrable objects, through a mapping that is designed to preserve the volume fraction occupied by the particle cores and the specific surface area. Results are presented for the mean value and standard deviation of the pore radius as functions of the rod aspect ratio, volume fraction, and polydispersity (degree of nonuniformity in the aspect ratios of the particles).

DOI: 10.1103/PhysRevE.93.062601

## I. INTRODUCTION

Quantitative models for the pore-size distribution play a central role in characterizing mobility [1], partitioning, and diffusion [2–6] in gels, fiber networks, and related sterically hindered environments. An early and influential result [7,8] in this area examined the case of randomly arranged fibers with lengths that were assumed to be very large relative to their diameter (or width) and that occupied infinitesimally small volume fractions. More recently, approaches have been developed [9,10] that extend the applicability of this finding to a wider range of volume fractions and that correctly predict mean values for the pore radii that vanish when the particle-occupied volume fraction approaches unity [11]. Recent works [12,13] have examined the case of rods of zero width (line segments) and finite, uniform lengths as the obstacles. Nevertheless, the approximations that fibers are of uniform dimensions (that is, are "monodisperse") and have very large (effectively infinite) aspect ratios are still frequently invoked. The present work describes a modeling framework that aims to relax these assumptions.

We consider a system of randomly arranged and isotropically oriented cylindrical fibers, where the lengths and radii of the particles follow a distribution function that we assume to be known. The (impenetrable) particles that comprise this system are then mapped onto a hypothetical, analogous system of fully penetrable monodisperse (uniform-sized) rods in a fashion that preserves (i) the volume fraction occupied by the cores of the particles, and (ii) the specific surface area per unit volume [11]. This analogy allows us to treat the volume fraction and specific surface area as the key microstructural variables and permits the development of a simple excluded-volume model that involves the mutually interpenetrable particles. Excluded-volume arguments applied to the steric interaction between a test sphere and the hypothetical, interpenetrable particles (that, however, are *not* permitted to overlap the test sphere) lead to an expression for the pore-size distribution function that accounts for polydispersity in the distribution over radii and lengths of the original system of impenetrable objects. It bears noting that although our formalism may appear to be nominally applicable to the full range of occupied volume fractions $0 \leqslant \phi \leqslant 1$, random systems of nonpenetrable particles exhibit random close packing (or jamming) at volume fractions that are smaller than unity and that depend upon the aspect ratio of the particles [14–16]. This threshold acts as an upper bound to the domain over which our results are applicable, and is relevant also for earlier, classical models for the pore size distribution. Our analysis follows lines similar to those developed in Ref. [11] for mixtures of rods and disks, with the present work focusing upon effects due to polydispersity and those arising out of the finite aspect ratio of real rod-like particles.

The specification of our model and our calculation of the pore-size distribution are presented in Secs. II A and II B, respectively, and our model for polydispersity is described in Sec. II C. Sections III and IV present results for the mean pore radius and standard deviation in the pore radii from calculations performed using the formalism of Sec. II, and concluding remarks, respectively.

## II. DISTRIBUTION OVER PORE SIZES IN A RANDOM ARRAY OF POLYDISPERSE RODS

### A. Specification of the model system

We consider a system of isotropically oriented and randomly distributed, impenetrable, cylindrical rods, with radii and lengths denoted by the symbols $R$ and $L$, respectively. The dimensions of the individual particles are described by the probability distribution function $\psi(R,L)$, which is normalized such that $\int_0^\infty dRdL\psi(R,L) = 1$, and moments over this distribution are denoted using the notation $\langle R^n L^m\rangle = \int_0^\infty dRdLR^n L^m \psi(R,L)$. The volume fraction occupied by the cores of the rods, denoted $\phi$, satisfies $\phi = \pi\rho\langle R^2 L\rangle$, where $\rho$ represents the overall number density of rods regardless of their length or radius. The pore-size distribution [denoted $f(r)$] is defined such that $f(r)dr$ equals the probability that a randomly chosen point located in the void space (that is, outside the impenetrable particle cores) is located at a distance within the range $(r, r+dr)$ from the surface of the nearest rod. We next consider a mapping of this system of polydisperse, impenetrable particles onto a hypothetical analogous system of fully mutually penetrable cylinders that are assumed to

*apchatte@esf.edu

 

have uniform (monodisperse) dimensions and to be oriented isotropically. The number densities, radii, and lengths that characterize the fully penetrable particles are denoted $\rho_0, R_0$, and $L_0$, respectively. A nondimensionalized density for the system of penetrable particles is introduced according to $\eta = \pi \rho_0 R_0^2 L_0$. The penetrable particles comprising the analogous, dual system are assumed to be located and oriented in a fully uncorrelated, random fashion.

The probability that a test sphere with radius denoted $r$ and centered at a randomly chosen point anywhere within the system of penetrable particles does *not* overlap *any* of the (mutually interpenetrable) rods equals [17]

$$K(r) = e^{-\rho_0 v}, \tag{1}$$

where $v$ denotes the orientationally averaged excluded volume between the test sphere and any of the penetrable rods and is given by [18,19]

$$v = \pi {R_0}^2 L_0 + \frac{4\pi r^3}{3} + 2\pi R_0 r(L_0 + R_0) + \pi r^2(\pi R_0 + L_0). \tag{2}$$

The pore-size distribution for the penetrable particle system is determined next from $K(r)$ and Eqs. (1) and (2). Following upon this step, the dimensions of the penetrable (subscript "0") particles will be related to those of the impenetrable (unsubscripted) particles by requiring that (i) the occupied volume fraction, and (ii) the surface area per unit volume, be equal for both the subscripted and unsubscripted systems. This (admittedly heuristic) formalism will lead to a closed form for the pore-size distribution that accounts for polydispersity and finite rod-length effects from a viewpoint that treats the volume fraction and specific surface area as the key microstructural descriptors.

### B. Determination of the pore-size distribution

Examination of the probability for no overlaps for the case of a test sphere of zero radius ($r \to 0$) using Eqs. (1) and (2) reveals that the volume fraction (denoted $\phi$) that is occupied by the cores of the penetrable particles (and thereby forbidden to the test sphere) is

$$K(r \to 0) = 1 - \phi = e^{-\pi \rho_0 {R_0}^2 L_0}, \tag{3}$$

which may also be written as

$$\eta = -\ln(1 - \phi) = \pi \rho_0 R_0^2 L_0. \tag{4}$$

Restriction of the choice location for the center of the test sphere to points that are within the free volume (thereby excluding the space that is actually occupied by the cores of the particles) requires modification of our result for $K(r)$ in Eq. (1) by a factor of $1(1 - \phi)$:

$$K_0(r) = \frac{K(r)}{(1 - \phi)} = e^{-\rho_0 v + \eta}. \tag{5}$$

Equations (2) and (5) yield

$$K_0(r) = e^{-A(r)}, \tag{6}$$

where

$$A(r) = \eta\left[\frac{4}{3}\left(\frac{r}{R_0}\right)^2\left(\frac{r}{L_0}\right) + 2\left(1 + \frac{R_0}{L_0}\right)\left(\frac{r}{R_0}\right) + \left(\frac{\pi R_0}{L_0} + 1\right)\left(\frac{r}{R_0}\right)^2\right]. \tag{7}$$

The pore-size distribution function, $f(r)$, is ascertained from Eqs. (6) and (7) as follows:

$$f(r) = -\frac{\partial K_0(r)}{\partial r} = \left(\frac{\partial A}{\partial r}\right)e^{-A(r)}, \tag{8}$$

where the function $A(r)$ is given by Eq. (7) and $f(r)$ satisfies the normalization relation: $\int_0^\infty dr f(r) = 1$. In our next step that completes the mapping, we relate the quantities $\eta, R_0$, and $L_0$ that characterize the penetrable particles to the variables that pertain to the impenetrable cylinders (which have been assumed to be polydisperse).

Equations (7) and (8) show that the specific surface area per unit volume for the system of penetrable particles is given by [17,20]

$$s_0 = (1 - \phi) \lim_{r \to 0} f(r) = \left(\frac{2}{R_0}\right)\eta(1 - \phi)\left(1 + \frac{R_0}{L_0}\right), \tag{9}$$

where $\phi$ represents the volume fraction occupied by the cores of the penetrable particles and is to be equated to the corresponding core-occupied volume fraction for the system of nonpenetrable objects. Corresponding to Eq. (9), the specific surface area for the system of polydisperse nonpenetrable rods is

$$s = \frac{2\phi[\langle RL\rangle + \langle R^2\rangle]}{\langle R^2 L\rangle}. \tag{10}$$

We next equate the specific surface areas from Eqs. (9) and (10) and use Eq. (4) to obtain the condition

$$\left(\frac{1}{R_0} + \frac{1}{L_0}\right) = \frac{\phi[\langle RL\rangle + \langle R^2\rangle]}{(1 - \phi)\eta\langle R^2 L\rangle}, \tag{11}$$

which we require to be satisfied for all permissible choices of the volume fraction and particle-size distribution function $\psi(R, L)$. Based upon the structure of Eq. (11), we adopt the following *ansatz* for $\rho_0, R_0$, and $L_0$:

$$R_0 = \eta\left(\frac{1 - \phi}{\phi}\right)\left(\frac{\langle R^2 L\rangle}{\langle RL\rangle}\right), \tag{12}$$

$$L_0 = \eta\left(\frac{1 - \phi}{\phi}\right)\left(\frac{\langle R^2 L\rangle}{\langle R^2}\right), \tag{13}$$

and

$$\rho_0 = \left(\frac{\phi}{1 - \phi}\right)^3\left(\frac{\langle RL\rangle^2\langle R^2\rangle}{\pi\eta^2\langle R^2 L\rangle^3}\right). \tag{14}$$

The choices made in Eqs. (12)–(14) ensure that for monodisperse systems, $R_0$ (or $L_0$) depends only upon $R$ (or $L$) and $\phi$ and is independent of $L$ (or $R$), and that as the volume fraction approaches zero each of the quantities $\rho_0, R_0$, and $L_0$ approaches $\rho, R$, and $L$, respectively. It also bears noting that the *ansatz* expressed by Eqs. (12)–(14) leads to a value for the aspect ratio of the hypothetical penetrable particles,

$L_0/R_0 = \langle RL\rangle/\langle R^2\rangle$, which is independent of the volume fraction.

Equations (4), (7), (8), and (12)–(14) yield the following expressions for the mean and mean-squared values for the pore-size distribution (following a step of integration by parts):

$$\frac{\langle r\rangle}{\langle R\rangle} = \frac{1}{\langle R\rangle}\int_0^\infty dr f(r) r = \left(\frac{\langle R^2 L\rangle}{\langle R\rangle\langle RL\rangle}\right) g(\phi)\int_0^\infty dx e^{-\eta B(R_0/L_0,x)}, \quad (15)$$

and

$$\frac{\langle r^2\rangle}{\langle R\rangle^2} = \frac{1}{\langle R\rangle^2}\int_0^\infty dr f(r) r^2 = 2\left(\frac{\langle R^2 L\rangle}{\langle R\rangle\langle RL\rangle}\right)^2 g^2(\phi)\int_0^\infty dx e^{-\eta B(R_0/L_0,x)} x, \quad (16)$$

where

$$g(\phi) = \frac{(1-\phi)\eta}{\phi}, \quad (17)$$

and

$$B\left(\frac{R_0}{L_0},x\right) = \frac{4}{3}\left(\frac{R_0}{L_0}\right)x^3 + \left(\frac{\pi R_0}{L_0}+1\right)x^2 + 2\left(1+\frac{R_0}{L_0}\right)x. \quad (18)$$

The variable of integration $x$ in Eqs. (15) and (16) represents $x = r/R_0$, where $r$ is the pore radius variable.

The results presented in Sec. III for rod systems with finite aspect ratios are obtained by numerical evaluation of the integrals that appear in Eqs. (15) and (16). However, in cases where the aspect ratios for all the rods are large enough that one may take the limit $R_0/L_0 \to 0$ in Eq. (18), that is when $\langle RL\rangle \gg \langle R^2\rangle$, the integrals in Eqs. (15) and (16) can be evaluated in closed form [21] to yield

$$\left.\frac{\langle r\rangle}{\langle R\rangle}\right|_{L\to\infty} = \left(\frac{\sqrt{\pi\eta}}{2\phi}\right)\left(\frac{\langle R^2 L\rangle}{\langle R\rangle\langle RL\rangle}\right)\mathrm{Erfc}(\sqrt{\eta}), \quad (19)$$

and

$$\left.\frac{\langle r^2\rangle}{\langle R\rangle^2}\right|_{L\to\infty} = \left(\frac{\langle R^2 L\rangle}{\langle R\rangle\langle RL\rangle}\right)^2\left(\frac{g^2(\phi)}{\eta}\right) \times [1-\sqrt{\pi\eta}e^{\eta}\mathrm{Erfc}(\sqrt{\eta})], \quad (20)$$

where $g(\phi)$ is defined in Eq. (17) and Erfc denotes the complementary error function. It can be verified from Eq. (17) that the function $g(\phi)$ decreases monotonically from unity to zero as $\phi$ increases from zero to unity. For the situation of monodisperse particles (for which $R$ and $L$ have unique values) with effectively infinite aspect ratios, Eqs. (19) and (20) reduce to the classic results derived by Ogston *et al.* [7,8] in the limit of vanishingly small volume fractions. Additionally, inspection of Eqs. (15)–(18) for the case of monodisperse rods shows that accounting for finite aspect ratio effects lowers the mean and mean-squared pore radii, namely, that if the volume fraction and $R$ are held fixed, systems with shorter rods will exhibit smaller values of $\langle r\rangle$ and $\langle r^2\rangle$.

### C. Modeling the impact of polydispersity

In considering the impact of polydispersity upon the first two moments of the pore radii we restrict our attention to the cases where the rods exhibit either (i) a distribution of lengths for a uniform value of the radius, or (ii) a distribution of radii for a uniform value of the length, in the interests of simplicity. Equations (12)–(18) reveal that in the most general case, the moments of $\psi(R,L)$ that control the pore radius distribution are $\langle R\rangle, \langle R^2\rangle, \langle RL\rangle$, and $\langle R^2 L\rangle$.

For a population of rods with a uniform hard-core radius $R$ but a distribution over the lengths $L$, we find from Eqs. (15)–(18) that for a fixed value of $R$, $\langle r\rangle$ and $\langle r^2\rangle$ are predicted to depend exclusively upon the volume fraction $\phi$ and the ratio $R/\langle L\rangle$. Increasing the mean aspect ratio $\langle L\rangle/R$ for a fixed volume fraction diminishes the function $B(R_0/L_0,x)$ of Eq. (18) for each fixed value of $x$, leading to (monotonically) larger values for both $\langle r\rangle$ and $\langle r^2\rangle$.

In the complementary case where the rods are assumed to be characterized by a uniform length $L$ but to have a distribution over their radii, it proves convenient to consider the normalized moments of the pore radii $\langle r\rangle/\langle R\rangle$ and $\langle r^2\rangle/\langle R\rangle^2$, as in Eqs. (15) and (16). Under these conditions, the normalized moments $\langle r\rangle/\langle R\rangle$ and $\langle r^2\rangle/\langle R\rangle^2$ are seen to depend upon the volume fraction, $L/\langle R\rangle$, and $\langle R^2\rangle/\langle R\rangle^2$. For concreteness, the calculations for which results are presented in Sec. III assume that the radii of the rods follow a Schulz distribution [17], namely that

$$\psi(R',L') = \delta(L'-L)\left(\frac{1}{\Gamma(m+1)}\right)\left(\frac{m+1}{\langle R\rangle}\right)^{m+1} \times R'^m e^{-(m+1)R'/\langle R\rangle}, \quad (21)$$

where the symbols $\delta$ and $\Gamma$ denote the Dirac delta function and Gamma function, respectively. The distribution of Eq. (21) is unimodal and is characterized by the quantities $\langle R\rangle$ and $m$, where the allowed range for $m$ is $0 \leqslant m \leqslant \infty$. In the limit that $m$ approaches infinity, Eq. (21) approaches a monodisperse Dirac delta function centered at $\langle R\rangle$, and when $m$ approaches zero Eq. (21) reduces to an exponential distribution. Moments of the Schulz distribution [Eq. (21)] are given by

$$\frac{\langle R^p\rangle}{\langle R\rangle^p} = \frac{\Gamma(p+m+1)}{(m+1)^p\Gamma(m+1)}, \quad (22)$$

which yields

$$m+1 = \langle R\rangle^2/{\sigma_R}^2, \quad (23)$$

where $\sigma_R$ denotes the standard deviation in the rod radii. (We similarly use the symbol $\sigma_r$ to denote the standard deviation in the pore radii, that is ${\sigma_r}^2 = \langle r^2\rangle - \langle r\rangle^2$). Given that the allowed range of values for $m$ is $0 \leqslant m \leqslant \infty$, Eq. (23) shows that for this choice of the distribution function $\psi(R,L)$, the standard deviation $\sigma_R$ is restricted to values that are no larger than the average rod radius $\langle R\rangle$. Figure 1 displays results for the pore-radius distribution function $f(r)$ calculated from Eqs. (7), (8), (12), and (13) for a system of rods that have uniform lengths but polydisperse radii. For fixed values of the volume fraction and average aspect ratio $L/\langle R\rangle$, the peak in the pore-size distribution moves toward larger radii and becomes broadened and flattened with increasing polydispersity in the

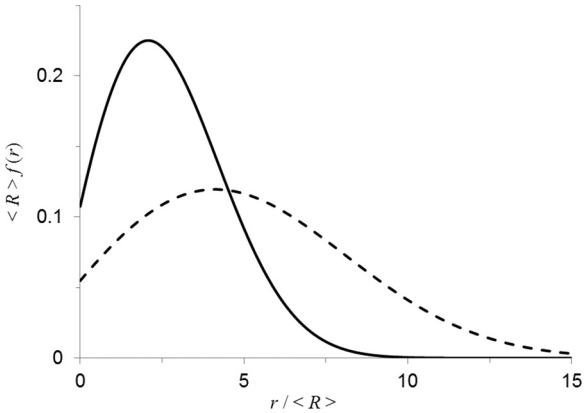


FIG. 1. The normalized pore radius distribution function calculated from Eqs. (7), (8), (12), and (13), $\langle R\rangle f(r)$, is shown as a function of $r/\langle R\rangle$ for rods with an aspect ratio $L/\langle R\rangle = 50$ and volume fraction $\phi = 0.05$. The solid and broken lines correspond to monodisperse rods ($\sigma_R =$ zero) and to polydisperse rods for which $\sigma_R = \langle R\rangle$, respectively. The mean value and standard deviation of the pore radii (calculated from Eqs. (15)–(18)) are equal to $\langle r\rangle/\langle R\rangle = 2.81$ and $\sigma_r/\langle R\rangle = 1.72$ for the monodisperse rods (solid line), and $\langle r\rangle/\langle R\rangle = 5.32$ and $\sigma_r/\langle R\rangle = 3.19$ for the polydisperse rods (broken line), respectively.

rod radii. These trends are manifested in concomitant increases in $\langle r\rangle/\langle R\rangle$ and $\sigma_r/\langle R\rangle$ with increasing polydispersity. Results from calculations of $\langle r\rangle/\langle R\rangle$ and $\sigma_r/\langle R\rangle$ as functions of the volume fraction, mean aspect ratio, and $\sigma_R/\langle R\rangle$ are presented in Sec. III.

## III. RESULTS

In presenting results for the mean pore radius and the standard deviation in pore radii as calculated from our model, we first consider the case of monodisperse rods for which $L$ and $R$ have unique values. Figures 2 and 3 display results for $\langle r\rangle/R$ and $\sigma_r/R$ as functions of $\phi$ and $\langle r\rangle/R$, respectively, for

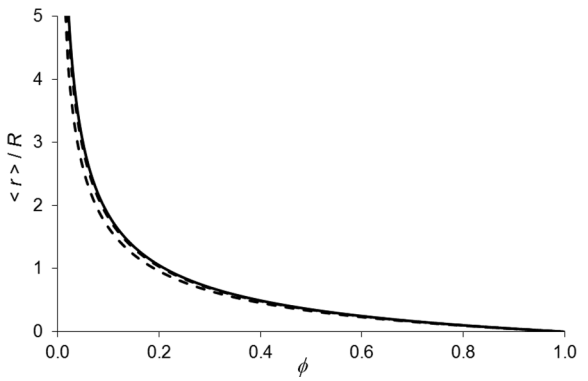


FIG. 2. The mean pore radius normalized by the rod radius, $\langle r\rangle/R$, is shown as a function of the volume fraction $\phi$ for monodisperse rods. The solid curve displays the result for the limiting case: $L/R \to \infty$ [Eq. (19)]. The lower and upper broken curves correspond to $L/R$ equal to 20 and 100, respectively, and are calculated from Eqs. (15), (17), and (18). The upper broken curve is nearly indistinguishable from the solid curve.

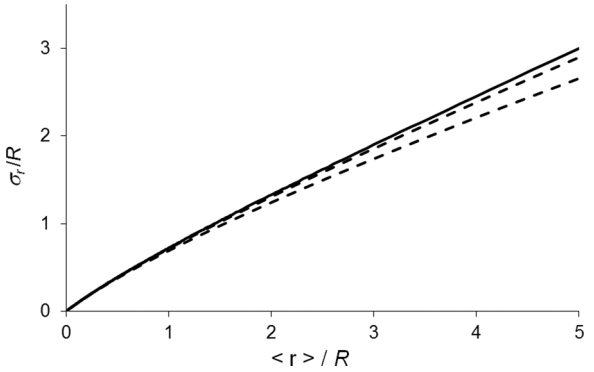


FIG. 3. The standard deviation in the radius normalized by the rod radius, $\sigma_r/R$, is shown as a function of the normalized mean pore radius $\langle r\rangle/R$ for monodisperse rods. The solid curve displays the result for the limiting case: $L/R \to \infty$ [Eqs. (19) and (20)]. The lower and upper broken curves correspond to $L/R$ equal to 20 and 100, respectively, and are calculated from Eqs. (15)–(18).

different fixed values of $R/L$. The broken lines in Figs. 2 and 3 are calculated from Eqs. (15)–(18); the solid lines represent the limiting case of monodisperse rods with infinite aspect ratios and are calculated from Eqs. (19) and (20). In Fig. 3, the volume fraction increases as we travel from right to left across the figure. For each fixed value of $R/L$, both $\langle r\rangle/R$ and $\sigma_r/R$ are found to be monotonically decreasing functions of the volume fraction $\phi$. As mentioned briefly in Sec. II C, increasing the aspect ratio (reducing $R/L$) for a fixed value of $\phi$ translates into larger values for the mean pore radius, in a trend that saturates when $L/R \approx 100$.

The physical basis for this effect arises from the circumstance that in order to achieve a given volume fraction with a

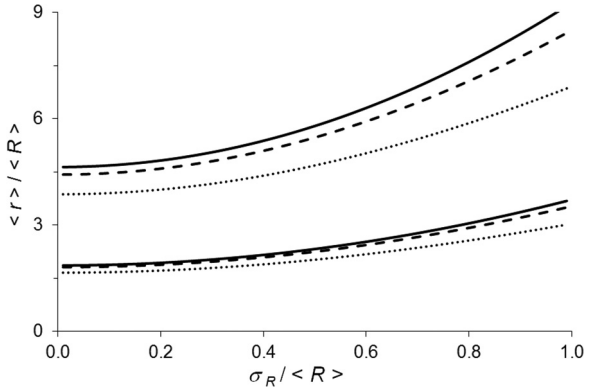


FIG. 4. The mean pore radius normalized by the average rod radius, $\langle r\rangle/\langle R\rangle$, for rods with uniform lengths and polydisperse radii, is shown as a function of the normalized standard deviation in the rod radii $\sigma_R/\langle R\rangle$. The rod radii are assumed to follow a Schulz distribution in each case. The upper and lower solid lines correspond to $L/\langle R\rangle \to \infty$ [Eq. (19)] for the fixed volume fractions $\phi = 0.025$ (upper) and $\phi = 0.1$ (lower), respectively. The upper and lower dashed lines correspond to $L/\langle R\rangle = 100$ [Eqs. (15)–(18)], for the fixed volume fractions $\phi = 0.025$ (upper) and $\phi = 0.1$ (lower), respectively. The upper and lower dotted lines correspond to $L/\langle R\rangle = 20$ [Eqs. (15)–(18)], for the fixed volume fractions $\phi = 0.025$ (upper) and $\phi = 0.1$ (lower), respectively.

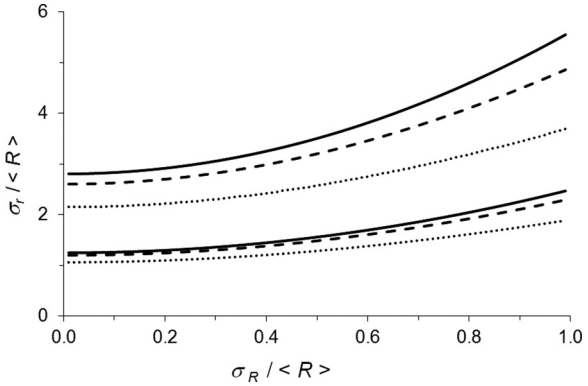


FIG. 5. The standard deviation of the pore radii normalized by the average rod radius, $\sigma_r/\langle R\rangle$, for rods with uniform lengths and polydisperse radii, is shown as a function of the normalized standard deviation in the rod radii $\sigma_R/\langle R\rangle$. The rod radii are assumed to follow a Schulz distribution in each case. The upper and lower solid lines correspond to $L/\langle R\rangle \to \infty$ [Eqs. (19) and (20)] for the fixed volume fractions $\phi = 0.025$ (upper) and $\phi = 0.1$ (lower), respectively. The upper and lower dashed lines correspond to $L/\langle R\rangle = 100$ [Eqs. (15)–(18)], for the fixed volume fractions $\phi = 0.025$ (upper) and $\phi = 0.1$ (lower), respectively. The upper and lower dotted lines correspond to $L/\langle R\rangle = 20$ [Eqs. (15)–(18)], for the fixed volume fractions $\phi = 0.025$ (upper) and $\phi = 0.1$ (lower), respectively.

population of longer rods, there must exist a smaller number density of rods per unit volume of the system. Thus, as the aspect ratio $(L/R)$ is increased, although the excluded volume between each individual rod and a test sphere of fixed radius also becomes larger, there are concomitantly fewer randomly located particles per unit volume that might overlap with the test sphere. This reduction in the number of independent and randomly arranged particles, each of which individually exhibits a larger excluded volume with respect to the test sphere, explains the increase in $\langle r\rangle/R$ with $L/R$ for fixed values of $\phi$ that is observed in Fig. 2. Similar arguments apply toward the behavior observed for $\sigma_r/R$ in Fig. 3.

The impact of polydispersity in the radii of the rods upon $\langle r\rangle/\langle R\rangle$ and $\sigma_r/\langle R\rangle$ for fixed value of $L/\langle R\rangle$ and $\phi$ is explored in Figs. 4 and 5. Each of the calculations in Figs. 4 and 5 is performed for a Schulz distribution [Eq. (21)] over the rod radii, and the rods are assumed to have uniform lengths $L$. The broken and solid lines in Figs. 4 and 5 are evaluated from Eqs. (15)–(18), and (19) and (20), respectively. For each case examined, increasing polydispersity in the rod diameters (quantified by $\sigma_R/\langle R\rangle$) leads to larger values for both $\langle r\rangle/\langle R\rangle$ and $\sigma_r/\langle R\rangle$ for fixed values of $L/\langle R\rangle$ and $\phi$. Larger values of $L/\langle R\rangle$ for fixed values of $\sigma_R/\langle R\rangle$ and $\phi$ correspond to increases in both $\langle r\rangle/\langle R\rangle$ and $\sigma_r/\langle R\rangle$, in a manner similar to that reported for monodisperse systems in Figs. 2 and 3. The sensitivity of both $\langle r\rangle/\langle R\rangle$ and $\sigma_r/\langle R\rangle$ toward changes in $L/\langle R\rangle$ decreases with increase in the volume fraction. A similar trend of increase in the mean pore radius with polydispersity in the dimensions of the obstacles has been reported in prior work that examined the situation of randomly located polydisperse spherical particles [17,22].

## IV. CONCLUDING REMARKS

A model has been developed for the pore-size distribution in systems of polydisperse rods with finite aspect ratios that exploits an analogy between systems of penetrable and impenetrable particles. It bears reiterating that our arguments ought to be viewed as entirely heuristic and motivated by the physical notion that the volume fraction and specific surface area are key microstructural descriptors, and that our development makes no pretense to be rigorous. Accounting for the finite nature of the rod aspect ratio is shown to reduce the mean pore radius when compared to that predicted for fibers with infinite aspect ratios at equal volume fractions. Additionally, polydispersity in the diameters of the rods is found to increase the expected mean pore radius, again under conditions of fixed volume fraction. When used in conjunction with implementations of the cell model [3,4], the present framework may prove to be useful for describing the impact of steric (excluded-volume) interactions upon diffusion and partitioning of tracer particles in realistic fiber networks [23]. Further development and analysis along the lines of this approach would also greatly benefit from appropriate computer simulation studies. It is hoped that our results encourage more such investigations that focus upon polydisperse systems.

[1] J. L. Viovy, Rev. Mod. Phys. **72**, 813 (2000).
[2] D. Rodbard and A. Chrambach, Proc. Natl. Acad. Sci. USA **65**, 970 (1970).
[3] B. Jonsson, H. Wennerstrom, P. G. Nilsson, and P. Linse, Colloid Polym. Sci. **264**, 77 (1986).
[4] L. Johansson, C. Elvingson, and J. E. Lofroth, Macromolecules **24**, 6024 (1991).
[5] M. J. Lazzara and W. M. Deen, J. Colloid Interface Sci. **272**, 288 (2004).
[6] J. C. Giddings, E. Kucera, C. P. Russell, and M. N. Myers, J. Phys. Chem. **72**, 4397 (1968).
[7] A. G. Ogston, Trans. Faraday Soc. **54**, 1754 (1958).
[8] A. G. Ogston, B. N. Preston, and J. D. Wells, Proc. R. Soc. Ser. A **333**, 297 (1973).
[9] J. C. Bosma and J. A. Wesselingh, J. Chromatogr. B **743**, 169 (2000).
[10] M. J. Lazzara, D. Blankschtein, and W. M. Deen, J. Colloid Interface Sci. **226**, 112 (2000).
[11] A. P. Chatterjee, J. Phys.: Condensed Matter **28**, 145301 (2016).
[12] C. Metzner, P. Krauss, and B. Fabry, arXiv:1110.1803v1 [q-bio.QM].
[13] N. R. Lang, S. Munster, C. Metzner, P. Krauss, S. Schurmann, J. Lange, K. E. Aifantis, O. Friedrich, and B. Fabry, Biophys. J. **105**, 1967 (2013).
[14] A. Donev, I. Cisse, D. Sachs, E. A. Variano, F. H. Stillinger, R. Connelly, S. Torquato, and P. M. Chaikin, Science **303**, 990 (2004).

[15] A. Donev, S. Torquato, F. H. Stillinger, and R. Connelly, J. Appl. Phys. **95**, 989 (2004).
[16] K. Desmond and S. V. Franklin, Phys. Rev. E **73**, 031306 (2006).
[17] S. Torquato, *Random Heterogeneous Materials: Microstructure and Macroscopic Properties* (Springer, New York, 2002).
[18] T. Kihara, Rev. Mod. Phys. **25**, 831 (1953).
[19] K. M. Jansons and C. G. Phillips, J. Colloid Interface Sci. **137**, 75 (1990).
[20] M. D. Rintoul, S. Torquato, C. Yeong, D. T. Keane, S. Erramilli, Y. N. Jun, D. M. Dabbs, and I. A. Aksay, Phys. Rev. E **54**, 2663 (1996).
[21] I. S. Gradshteyn and I. M. Ryzhik, *Table of Integrals, Series, and Products*, edited by A. Jeffrey (Academic Press, London, 1994).
[22] B. Lu and S. Torquato, Phys. Rev. A **45**, 5530 (1992).
[23] J. S. Meth, S. Gam, J. Choi, C. C. Lin, R. J. Composto, and K. I. Winey, J. Phys. Chem. B **117**, 15675 (2013).